On the other hand, the galena [110] direction is preferred by oxidation reaction fronts (Figs. 1 and 2), and a direct coupling of the sorption and reduction of aqueous Au with the initial oxidation of surface sulfide sites could produce the nucleation and growth of small Au clusters in this direction. We propose that such clusters grow and coalesce to form ordered domains within [110]-trending Au islands, as observed. It is likely that Au islands also grow by the diffusion of reduced Au along the galena surface to growing Au clusters. In either case, Au reduction is probably accompanied by polysulfide (S_x^{2-}) formation and Pb release into solution, with eventual formation and release of SO_4^{2-} (*18*). On preoxidized surfaces, similar mechanisms produce Au islands, except that there is little to no direct Au deposition on unoxidized surface sites. Thus, the oxidized galena surface exerts little influence on the shape and orientation of Au islands, and the rate of reaction is reduced by a factor of about 3.

We have extended previous studies of aqueous Au deposition on sulfides to show that surface oxidation, as well as oxidation-related Au deposition, are governed by surface structure to a degree that depends on the history of the surface. Further studies using scanning probe microscopes and other surface-sensitive techniques will add to our understanding of sulfide oxidation kinetics and mechanisms. Such knowledge will prove useful not only for understanding certain aspects of ore-forming processes, but it should also be applicable to ore-processing methods and to the environmental chemistry of sulfides.

REFERENCES AND NOTES

1. B. M. Bakken, M. F. Hochella, Jr., A. F. Marshall, A. M. Turner, *Econ. Geol.* **84**, 171 (1989); B. M. Bakken, thesis, Stanford University (1990).
2. G. M. Bancroft and M. M. Hyland, in *Mineral-Water Interface Geochemistry, Reviews in Mineralogy 23*, M. F. Hochella, Jr., and A. F. White, Eds. (Mineralogical Society of America, Washington, DC, 1990), chap. 13; A. Starling, J. M. Gilligan, A. H. C. Carter, R. P. Foster, R. A. Saunders, *Nature* **340**, 298 (1989).
3. STM imaging and spectroscopy were accomplished with the use of a Digital Instruments Nanoscope II equipped with an electrically isolated sample stage and tungsten tips etched in 1 M KOH. All surfaces used in this study were galena (100) cleavage planes exposed by fracture in air and either used immediately or allowed to age in air for several months (the latter are referred to as preoxidized surfaces). Galena has the NaCl structure and a bulk band gap of 0.4 eV, although the surface band gap is probably considerably less.
4. J. A. Tossell and D. J. Vaughn, *Can. Mineral.* **25**, 381 (1987).
5. M. F. Hochella Jr., *et al.*, *Am. Mineral.* **74**, 1233 (1989); M. F. Hochella, Jr., in *Mineral-Water Interface Geochemistry, Reviews in Mineralogy 23*, M. F. Hochella, Jr., and A. F. White, Eds. (Mineralogical Society of America, Washington, DC, 1990), chap. 3.
6. N. J. Zheng *et al.*, *Phys. Rev. B* **38**, 12780 (1988).
7. I. H. Wilson, N. J. Zheng, U. Knipping, I. S. T. Tsong, *Appl. Phys. Lett.* **53**, 2039 (1988); T. G. Sharp, N. J. Zheng, I. S. T. Tsong, P. R. Busek, *Am. Mineral.* **75**, 1438 (1990).
8. G. F. Cotterill, R. Bartlett, A. E. Hughes, B. A. Sexton, *Surf. Sci. Lett.* **232**, L211 (1990).
9. C. M. Eggleston and M. F. Hochella, Jr., *Geochim. Cosmochim. Acta* **54**, 1511 (1990).
10. A. N. Buckley and R. Woods, *Appl. Surf. Sci.* **17**, 401 (1984).
11. J. R. Gardner and R. Woods, *J. Electroanal. Chem.* **100**, 447 (1979).
12. PES shows evidence for chemisorption of O species (O_2, OH^-, H_2O, CO_2) within 1 min of exposure to air or water but no detectable sulfide oxidation for up to a day in air (*10*).
13. We use polyphenyl ether, a nonpolar, high molecular weight oil that has been utilized in other STM studies (*9*) and is not seen in STM images.
14. G. E. Jean and G. M. Bancroft, *Geochim. Cosmochim. Acta* **49**, 979 (1985).
15. For $d\ln I/d\ln V$ spectroscopy, 10 to 50 spectra were averaged and the feedback loop was run for 300 μs between individual spectra collections to stabilize the tip-sample separation. Tip stabilization was crucial to avoid tip crashes during data collection.
16. R. M. Feenstra, *J. Vac Sci. Technol. B* **7**, 925 (1989).
17. O. M. Magnussen, J. Hotlos, R. J. Nichols, D. M. Kolb, R. J. Behm, *Phys. Rev. Lett.* **64**, 2929 (1990); S. Manne, P. K. Hansma, J. Massie, V. B. Elings, A. A. Gewirth, *Science* **251**, 183 (1991).
18. M. M. Hyland and G. M. Bancroft, *Geochim. Cosmochim. Acta* **53**, 367 (1989).
19. We thank B. Bakken, G. Brown, G. Parks, V. Elings, J. Peck, C. Lang, S. Strauss, S. Stipp, P. Johnsson, and D. Coulman for helpful discussions, assistance, or materials. The Center for Materials Research at Stanford University provided financial and instrumental support. This work was also supported by grants from the Petroleum Research Fund (administered by the American Chemical Society) and the National Science Foundation (grants PRF 22892-AC5,2 and EAR-9105000, respectively, both to M.F.H.).

13 May 1991; accepted 13 August 1991

Hydrogen-Helium Mixtures at Megabar Pressures: Implications for Jupiter and Saturn

J. E. KLEPEIS,* K. J. SCHAFER, T. W. BARBEE III, M. ROSS

Models of Jupiter and Saturn postulate a central rock core surrounded by a fluid mixture of hydrogen and helium. These models suggest that the mixture is undergoing phase separation in Saturn but not Jupiter. State-of-the-art total energy calculations of the enthalpy of mixing for ordered alloys of hydrogen and helium confirm that at least partial phase separation has occurred in Saturn and predict that this process has also begun in Jupiter.

PLANETARY MODELS ARE CONSTRUCTED on the basis of observed characteristics such as the total mass, radius, rotation rate, and gravitational field of the planet. These measured quantities plus observations of the planetary atmospheres of Jupiter and Saturn are consistent with a hydrogen-helium mixture composed of 7% helium by number (23% by weight, the solar abundance) surrounding a central rock core (*1*). On the basis of these inputs, planetary evolution models can be used to determine the thermodynamic conditions as a function of time in the interior of the planet. The maximum temperature and pressure in the mixture occurs at the central core boundary; the best estimates for the current values are 45 Mbar and 20,000 K for Jupiter and 10 Mbar and 10,000 K for Saturn (*1*).

Evolutionary models also can be used to determine the energy output of the planet as a function of time. These models yield a cooling rate for Jupiter that is consistent with both its measured energy output and the approximate age of the solar system, but the corresponding rate for Saturn is too fast (*1–3*). It has been suggested (*4*) that, as the planets cooled, a temperature might have been reached at some distance from the central core at which helium-rich droplets would condense out of the hydrogen-helium mixture (phase-separate), releasing gravitational energy as they settled. This extra source of energy might then account for the anomalously slow cooling of Saturn. However, it has been assumed that this process has not occurred in Jupiter (*1, 2*). Thus far, the only internal energy source included in evolutionary models is the heat generated as a result of the gravitational collapse that occurred during the formation of the planet (*1*). Calculations including the possibility of phase separation have yet to be carried out [Stevenson and Salpeter (*2*) have discussed the detailed implications of phase separation but in general terms only]. A crucial ingredient in these calculations will be the pressure and temperature dependence of the miscibility gap in the hydrogen-helium mixture. In the calculations presented here we use state-of-the-art total energy (TE) methods to address this question.

At the pressures in the interiors of Jupiter and Saturn, hydrogen is believed to be a liquid metal (*5*) whereas helium should be

---

University of California, Lawrence Livermore National Laboratory, Livermore, CA 94550.

*To whom correspondence should be addressed.

an insulator with a wide band gap (*6*). However, most previous calculations for hydrogen-helium mixtures start with a fully pressure-ionized system of ions and include the response of the electron gas using perturbation theory (*7–9*). Using this approach, Stevenson (7) predicted that a 7% helium mixture would phase-separate at approximately 7000 K near 8 Mbar. Subsequently, a number of workers (*8, 9*) carried out classical Monte Carlo simulations for hydrogen-helium ionic mixtures. Those of Hubbard and DeWitt (*9*) yield a phase-separation temperature of approximately 7500 K near 8 Mbar for a planetary mixture. These two calculations support the view that phase separation has occurred in Saturn, at some distance from the central core, but not in Jupiter, because of its higher internal temperatures. However, MacFarlane (*10*) predicted that hydrogen-helium mixtures would not phase-separate at any temperature for pressures near 10 Mbar. He used a model potential extracted from Thomas-Fermi-Dirac calculations for alloys of hydrogen and helium in body-centered cubic (bcc) and face-centered cubic (fcc) crystal structures.

The crude treatment of the electronic structure in these previous calculations and the wide range in their predictions for the phase-separation temperature of a planetary mixture (0 to 7500 K) force the conclusion that these models were too inaccurate to determine whether phase separation has occurred in Jupiter and Saturn. The primary reason for this circumstance is that the relevant pressure range requires an accurate description of both nearly free hydrogen electrons and more tightly bound helium electrons in the same calculation. Although perturbative and Thomas-Fermi methods are not able to solve this difficulty, the state-of-the-art TE methods used in condensed matter theory offer the possibility of an accurate description of both constituents. The accuracy of these methods, which are based on the local density approximation (LDA) (*11*), is well established (*12*). The electrons are treated quantum mechanically in a one-electron approximation where each electron feels the Coulomb potential of the classical nuclei as well as the self-consistent potential from all of the remaining electrons. The biggest strength of TE methods is in determining the TE difference between two structures, where most of the errors due to the LDA cancel out. As a result of this cancellation, TE differences can have an accuracy as high as 0.05 eV, which corresponds to only 600 K. Our calculations apply these TE methods to high-pressure mixtures of hydrogen and helium.

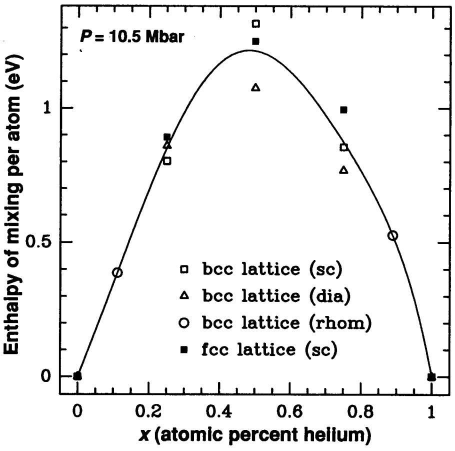

Fig. 1. The enthalpy of mixing per atom (defined in Eq. 1) obtained from TE calculations at a pressure of 10.5 Mbar and a temperature of 0 K. The symbols at specific values of x (number fraction of helium atoms) correspond to different ordered alloys in bcc and fcc crystal structures. The label sc refers to the calculations carried out for a simple cubic unit cell in both bcc (two atoms per cell) and fcc (four atoms per cell) lattices. Similarly, dia refers to a bcc lattice with a diamond-like unit cell consisting of four atoms arranged along the (111) direction. For each of these structures, calculations were carried out for all of the distinct atomic configurations. The label rhom refers to a bcc structure with a rhombohedral unit cell that contains a single atom of one type and its eight bcc nearest neighbors of the opposite type. The curve is a polynomial fit to both the bcc and the fcc calculations [the precise form is given in (*13*)].

The primary result of our TE calculations [a more detailed account of the method and results will be published separately (*13*)] is given in Fig. 1, which shows the enthalpy of mixing per atom at 0 K and 10.5 Mbar,

$$\Delta H(x) = H(x) - xH(x = 1) - (1 - x)H(x = 0) \qquad (1)$$

where $H(x) = E(x) + PV(x)$ is the enthalpy per atom and x is the number fraction of helium atoms [$E(x)$ is the total energy per atom; P is the pressure, which is held constant; and $V(x)$ is the volume per atom]. The variation in the results for different bcc and fcc structures (Fig. 1) reflects the dependence on atomic configuration [a more detailed description of the structures is given in (*13*)].

The ionic zero-point energy contribution to ΔH has been neglected, but a simple estimate (*13*) indicates that it is an order of magnitude smaller than the electronic energy. From Fig. 1, we see that the energy cost is larger to substitute a small amount of hydrogen in a lattice of helium than to substitute a small amount of helium in a lattice of hydrogen. In addition, we find that the approximation of additive volumes,

$$V(x) \approx xV(x = 1) + (1 - x)V(x = 0) \qquad (2)$$

all at constant pressure, is accurate to about 1% for alloys of hydrogen and helium. This result implies that the large values of ΔH in Fig. 1 are due to the total energy contribution, the $P\Delta V$ term being small. In their Monte Carlo simulations Hubbard and DeWitt (*9*) found this same result, which bears on the determination of the helium abundances in the interiors of Jupiter and Saturn (*1, 2*).

The calculated ΔH is a very slowly varying function of pressure. For all of the alloys considered, $\Delta H(x)$ is virtually unchanged between 5 and 10 Mbar. In addition, we find (*13*) that $\Delta H(x = 1/2)$ in the bcc-sc structure is nearly constant between 5 and 20 Mbar and that above 20 Mbar it decreases very slowly with increasing pressure (it has dropped by only 35% at 1000 Mbar). In our calculations pure helium metallizes at slightly less than 40 Mbar in the bcc structure (the energy gap between the 1*s* band and the 2*p* band goes to zero). However, we find that nothing striking happens to ΔH at 40 Mbar; it is still large (for $x = 1/2$ in the bcc-sc structure it has dropped by only 10% from the value at 5 Mbar) at this pressure and remains large at higher pressures. Even though helium is metallic at 40 Mbar, it is a very "poor" metal in the sense that the density of states at the Fermi level is small. Thus it may not be surprising that at this pressure helium is still immiscible in hydrogen, which is a very "good" free-electron–like metal. The metallization of pure helium occurs because the electronic states become more free-electron–like as the pressure is increased. This same trend causes ΔH to be small at sufficiently high pressures, but the exact point at which pure helium metallizes is unimportant. The accu-

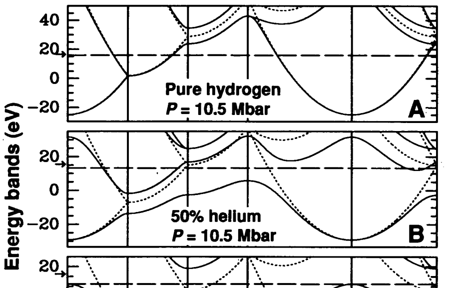

Fig. 2. The energy bands along high symmetry lines for the bcc-sc structure (with the unit cube as the primitive cell—two atoms per cell). The solid lines are the bands obtained from the TE calculations and correspond to a pressure of 10.5 Mbar; the dotted lines are the purely free-electron bands at the same volumes. The horizontal dashed lines indicate the accurate Fermi level, and the small arrows at the left indicate the free-electron Fermi level. (**A**) Bands for pure hydrogen, (**B**) bands for the bcc-sc alloy containing 50% helium, and (**C**) bands for pure helium.

rate treatment of the electronic structure in our TE calculations, which was missing in previous treatments, has allowed us to demonstrate this point.

An analysis of the electronic band structures obtained from the TE calculations [a detailed discussion is given elsewhere (*13*)] yields a number of important insights. If the accurate bands in Fig. 2 (solid lines) were exactly free-electron–like (dotted lines) for the alloy as well as for the pure constituents, then there would be no distinction between hydrogen electrons and helium electrons and so we would expect ΔH to be small. However, the TE calculations (Fig. 1) find a large ΔH and therefore the deviations from the free-electron bands must be important, because the electronic energy is the dominant contribution to ΔH. The bands for pure hydrogen are very close to the free-electron bands, especially below the Fermi level (Fig. 2A). However, there are significant deviations from the free-electron bands for the alloy (Fig. 2B) and the deviations for pure helium are similar in magnitude to the bandwidths (Fig. 2C). In view of these large deviations, it is likely that any perturbation theory treatment starting with free-electron states will break down for the helium-derived electronic states. This result calls into question the conclusions of previous calculations (*7–9*), which were based on perturbation theory.

For the 50% bcc-sc alloy (Fig. 2B) there are two distinct bands, one that is entirely below the Fermi level and another that intersects the Fermi level at several points in the Brillouin zone. Examining the orbital character of these two bands, we find that the lower band is composed primarily of the helium 1*s* orbital with only a small admixture of hydrogen 1*s*. Similarly, the band that intersects the Fermi level is composed primarily of the hydrogen 1*s* orbital with only a small admixture of helium 1*s*. This separation into a hydrogen band and a helium band is due to the fact that the helium-derived electrons are more tightly bound to the helium nuclei and therefore are at lower energies relative to the hydrogen-derived electrons. This energy separation inhibits the formation of the alloy (*13*) and must be treated accurately in order to obtain correct results for ΔH. This conclusion is the most fundamental result of our TE calculations. Calculations based on perturbation theory yield incorrect energies for the formation of a hydrogen-helium mixture because their inaccurate description of the electronic states leads to an underestimate of the energy separation between the hydrogen and helium electrons. We also find that the widths of the hydrogen and helium bands must be much larger than the energy difference between the hydrogen and helium electrons before ΔH becomes small (that is, the pressure must be very high). This fact explains why our ΔH decreases so slowly with pressure.

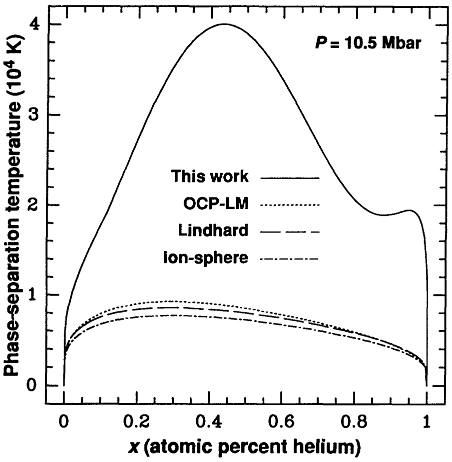

Fig. 3. The solid curve is our calculation of the phase-separation temperatures at a pressure of 10.5 Mbar (based on the results of TE calculations and Eq. 3). The critical (maximum) temperature is estimated to be T_c = 40,000 ± 12,000 K at a critical concentration of x_c = 0.43. We also find the phase-separation temperature at x = 0.07 (relevant to Jupiter and Saturn) to be T = 15,000 ± 3,000 K. The uncertainties arise from both the limited number of atomic configurations we consider and our simplified treatment of thermal effects. The remaining curves are obtained from three different plasma models (see text).

The relatively large, positive values of ΔH in Fig. 1 imply that a high temperature must be reached before entropy dominates and the fully mixed phase becomes energetically favored over the coexistence of a helium-rich phase and a helium-poor phase. In order to directly address the question of phase separation, we construct a simple model that extends our TE calculations to nonzero temperatures. From the energy bands in Fig. 2 we see that the Fermi energy of the electrons (the energy difference between the lowest band at Γ and the Fermi level) is on the order of 40 eV. Because the temperatures of interest correspond to $k_B T \approx 1$ eV and ΔH is dominated by the electronic energy, it is reasonable to assume that ΔH is independent of temperature T in this range (we neglect the contribution from the lattice dynamics). The second, and more crucial, approximation is that we consider only the ideal entropy of mixing. With these two assumptions we can calculate the Gibbs free energy of mixing,

$$\Delta G(x) = \Delta H(x) + k_B T[x \ln x + (1-x)\ln(1-x)] \quad (3)$$

where k_B is the Boltzmann constant.

Through a series of common tangent constructions (*13*) we can determine the phase-separation temperature for all values of x. The results of this calculation, at a pressure of 10.5 Mbar, are shown as the solid curve in Fig. 3. This curve indicates that more than two phases can coexist in a small range of temperatures around 19,000 K. There is a large uncertainty in our calculation of the phase-separation temperatures because we obtained the ΔH contribution to ΔG by fitting only a small number of points. In order to estimate this uncertainty, we calculated the phase-separation temperatures on the basis of fits of ΔH to different subsets of the structures shown in Fig. 1. The solid curve in Fig. 3 is based on the fit of ΔH shown in Fig. 1. Using this fit, we find a critical (maximum) phase-separation temperature of T_c = 40,000 ± 10,000 K at a critical concentration of x_c = 0.43. We also find the phase-separation temperature at x = 0.07 (relevant to Jupiter and Saturn) to be T = 15,000 ± 2,000 K. These uncertainties are due only to the limited number of atomic configurations we consider and do not include those due to our simplified treatment of thermal effects, which we estimate next. We emphasize that the uncertainties from both of these sources are larger than the small uncertainties in the TE calculations themselves.

We can estimate the additional uncertainty arising from our simplified treatment of thermal effects by a comparison with plasma models for which the equation of state of the solid and fluid are known accurately. The fluid plasma models include the contribution from the lattice dynamics and properly account for the disordered nature of the fluid. Conversely, the solid plasma models neglect the lattice dynamics and assume a perfect crystalline lattice, just as we have done. We first calculate the phase-separation temperatures, at a pressure of 10.5 Mbar, by applying the linear-mixing (LM) model (*14*) to a fit of the Helmholtz free energy obtained from the Monte Carlo simulations of Stringfellow *et al.* (*15*) for the one-component plasma (OCP). These results are plotted as the dotted curve in Fig. 3 (labeled OCP-LM). We next consider the ion-sphere model (*16*), which makes essentially the same approximations for the ion-ion interaction as in the OCP-LM calculation but includes thermal effects exactly as we do in Eq. 3. The phase-separation temperatures for this model, at 10.5 Mbar, are plotted as the dot-dashed line in Fig. 3 (labeled ion-sphere). The difference between the ion-sphere and OCP-LM curves at x = 0.07 is very close to 1000 K, and the corresponding difference in the critical temperature is approximately 2000 K. We take these quantities to be estimates of the uncertainty due to the simplified treatment of thermal effects in our calculation (the neglect of lattice dynamics and the use of perfect crystalline lattices). Both plasma models may be compared to the Monte Carlo simulations of Hubbard and DeWitt (*9*) (at 10.5 Mbar), who used the Lindhard dielectric function to screen the bare Coulomb interaction between the ions (dashed curve in Fig. 3 labeled Lindhard). The Lindhard results are very close to both the OCP-LM and ion-sphere curves but very far from our calculations.

Our phase-separation temperatures were calculated for a pressure of 10.5 Mbar but are virtually independent of pressure in the range from 5 to 20 Mbar. However, at low pressures hydrogen is a molecular insulator and becomes a molecular metal near 2 Mbar (*5*). Van den Bergh and Schouten (*17*), using pair potentials fit to low-pressure experiments, found that for pressures up to 1 Mbar helium will be completely miscible in insulating, molecular hydrogen for temperatures above approximately 2500 K. The miscibility of helium in metallic, molecular hydrogen is unknown. Our calculations do not apply directly to this molecular phase, but in analogy with the metallization of pure helium we expect that the precise pressure at which molecular hydrogen metallizes will be unimportant with regard to the miscibility. Rather, we expect that the phase-separation temperatures will increase monotonically from van den Bergh and Schouten's values at 1 Mbar to the values we calculate at sufficiently high pressure, where hydrogen is an atomic (rather than molecular) metal. Additional TE calculations for alloys containing molecular hydrogen are needed in order to accurately determine the behavior of the miscibility gap below 5 Mbar.

The primary conclusion obtained from the results of our TE calculations is that it is crucial to treat the electronic structure accurately in order to obtain the correct thermodynamics for hydrogen-helium mixtures at megabar pressures. The electronic energy makes a large contribution to the phase-separation temperature. This temperature could be small only if we have severely underestimated the thermal contribution. Barring this circumstance, our phase-separation temperature of 15,000 ± 3,000 K for a 7% helium mixture confirms that the fluid interior of Saturn has at least partially phase-separated, because the maximum temperature in the fluid is estimated to be only 10,000 K. The estimated temperatures in the fluid interior of Jupiter range from 10,000 K near the surface to 20,000 K at the central core (*1*). Thus our calculation predicts that phase separation has also begun in Jupiter. In view of this prediction, the fact that the currently successful evolutionary models of Jupiter do not need to invoke phase separation may indicate a failure of these models. Alternatively, phase separation may have occurred too late in the evolution of Jupiter to provide a significant internal energy source up to the present time. In either case, new evolutionary calculations are needed to resolve this dilemma and to confirm that the inclusion of phase separation leads to a consistent model of Saturn.

REFERENCES AND NOTES

1. A. S. Grossman, J. B. Pollack, R. T. Reynolds, A. L. Summers, H. C. Graboske, *Icarus* **42**, 358 (1980); D. J. Stevenson, *Annu. Rev. Earth Planet. Sci.* **10**, 257 (1982).
2. D. J. Stevenson and E. E. Salpeter, *Astrophys. J. Suppl. Ser.* **35**, 221 (1977); *ibid.*, p. 239.
3. R. A. Hanel, B. J. Conrath, V. G. Kunde, J. C. Pearl, J. A. Pirraglia, *Icarus* **53**, 262 (1983).
4. R. Smoluchowski, *Nature* **215**, 691 (1967); E. E. Salpeter, *Astrophys. J.* **181**, L83 (1973).
5. T. W. Barbee III, A. Garcia, M. L. Cohen, J. L. Martins, *Phys. Rev. Lett.* **62**, 1150 (1989).
6. D. A. Young, A. K. McMahan, M. Ross, *Phys. Rev. B* **24**, 5119 (1981).
7. D. J. Stevenson, *ibid.* **12**, 3999 (1975).
8. E. L. Pollock and B. J. Alder, *Phys. Rev. A* **15**, 1263 (1977); J. P. Hansen, G. M. Torrie, P. Vieillefosse, *ibid.* **16**, 2153 (1977).
9. W. B. Hubbard and H. E. DeWitt, *Astrophys. J.* **290**, 388 (1985).
10. J. J. MacFarlane, *ibid.* **280**, 339 (1984).
11. See, for example, R. O. Jones and O. Gunnarsson, *Rev. Mod. Phys.* **61**, 689 (1989).
12. See, for example, J. DeVreese Ed., *Electronic Structure, Dynamics, and Quantum Structural Properties of Condensed Matter* (Plenum, New York, 1985).
13. J. E. Klepeis, K. J. Schafer, T. W. Barbee III, M. Ross, *Phys. Rev. B*, in press.
14. B. Brami, J. P. Hansen, F. Joly, *Physica A* **95**, 505 (1979); S. Ichimaru, H. Iyetomi, S. Ogata, *Astrophys. J.* **334**, L17 (1988).
15. G. S. Stringfellow, H. E. DeWitt, W. L. Slattery, *Phys. Rev. A* **41**, 1105 (1990).
16. E. E. Salpeter, *Aust. J. Phys.* **7**, 373 (1954).
17. L. C. van den Bergh and J. A. Schouten, *J. Chem. Phys.* **89**, 2336 (1988).

18. We are grateful to M. van Schilfgaarde for providing the linear muffin-tin orbital (LMTO) computer codes used in the calculations. We also acknowledge helpful discussions with A. K. McMahan. This work was performed under the auspices of the U.S. Department of Energy by the Lawrence Livermore National Laboratory under contract W-7405-ENG-48.

8 July 1991; accepted 22 August 1991

Superconductivity in the Fullerenes

C. M. Varma, J. Zaanen, K. Raghavachari

Intramolecular vibrations strongly scatter electrons near the Fermi-surface in doped fullerenes. A simple expression for the electron-phonon coupling parameters for this case is derived and evaluated by quantum-chemical calculations. The observed superconducting transition temperatures and their variation with lattice constants can be understood on this basis. To test the ideas and calculations presented here, we predict that high frequency H_g modes acquire a width of about 20% of their frequency in superconductive fullerenes, and soften by about 5% compared to the insulating fullerenes.

THE EXCITING DISCOVERY OF SUPERconductivity in metallic fullerenes (*1*) leads us to inquire whether the classic mechanism for superconductivity, namely, effective electron-electron attraction via the interaction of electrons with vibrations of the ions, is applicable here as well. Associated with this is the question of whether the direct electron-electron repulsion in Fullerenes can suppress conventional singlet pairing. In this paper we exploit the special nature of cluster compounds to derive a particularly simple expression for electron-vibrational coupling from which parameters of the superconducting state of fullerenes are easily calculated. Further, we present arguments why the effective repulsions in fullerenes are no different than in conventional metals.

The lattice vibrations couple to the electronic states of metallic fullerenes in two ways: by causing fluctuations in the hopping rate of electrons from one molecule to the other and by causing fluctuations in the electronic structure of a single molecule. The covalent interactions that split the molecular states, which form the bands in the metallic state, are over an order of magnitude larger than the inter-molecular covalency. This is reflected in the intra-molecular splitting $W_{\text{intra}} \simeq 20$ eV (*2, 3*) compared to the width of the t_{1u} bands which is $W_{\text{inter}} \simeq 0.6$ eV (*4, 5*). The electron-vibration coupling is known to be proportional to such covalent splittings (*6*). Therefore, in the problem of the fullerenes, one needs to consider only the intra-molecular vibration coupling. The same argument rationalizes why the electron-vibrational coupling may be much larger in doped fullerenes than in doped graphite. In the latter, the orbitals near the Fermi-energy are π bonded. The Fullerenes have a significantly larger relevant bandwidth, because of σ admixture due to the non-planar local geometry, and therefore a stronger

---

AT&T Bell Laboratories, Murray Hill, NJ 07974.